EUROPEAN JOURNAL OF COMPUTATIONAL MECHANICS, 2016
VOL. 25, NO. 3, 294–308
http://dx.doi.org/10.1080/17797179.2016.1212628

Taylor & Francis
Taylor & Francis Group

Mathematical framework for predicting the thermal behaviour of spectrally selective coatings within an industrial near-infrared furnace

D. A. Brennan[a], I. Mabbett[a], J. Elvins[b], N. P. Lavery[a] and D. A. Worsley[a]

[a]College of Engineering, Swansea University, Bay Campus, Swansea, UK; [b]Tata Steel, SPECIFIC, Baglan Bay Innovation Centre, Port Talbot, UK

ABSTRACT

A transient finite difference thermal model based on the heat equations is developed, valid for spectrally selective surface coatings on any substrate material within a near-infrared (NIR) furnace. Spectral radiative heat transfer equivalent to a blackbody provides the heat source. Both radiative and natural convective cooling are accounted for. A Monte Carlo ray tracing algorithm is formulated and used to determine the radiation view factor. The variance of the algorithm in relation to mesh resolution and sample size is tested against published exact solutions. The radiative flux is divided into absorbed and reflected bands using hemispherical reflectance spectra measured within the 250–15,000 nm wavelength range, enabling the model to predict the thermal build-up of coatings with very different radiative properties. Results show that the transient temperature distribution of spectrally selective surface coatings within an NIR furnace can be modelled, with good agreement observed between experimental and simulated data. The model shows the expected relationship between colour and absorption, with darker coatings displaying greater absorption and heating rates than lighter coatings. Surprisingly, colours which appear similar to one another can display different heating rates, a result of their varied infrared reflectance properties.

ARTICLE HISTORY
Received 4 October 2015
Accepted 5 July 2016

KEYWORDS
Applied mathematics; radiative heat transfer; Monte Carlo simulation; near-infrared heating; spectrally selective coatings; pre-painted steels

1. Introduction

Pre-painted steel products are widely used in the construction industry as effective materials for roofing and cladding systems. A typical product consists of mild steel substrate to which a functional coating system comprised of metallic and organic layers is applied. Metallic coatings are primarily zinc or zinc–aluminium-based alloys that provide sacrificial and barrier corrosion protection. A wide range of organic coatings are available, with PVC plastisol, PVDF, polyurethane

CONTACT D. A. Brennan brennanda@physics.org

and polyester systems being most suited to construction applications. Organic coatings, in addition to providing added barrier corrosion protection and aesthetics, are often formulated to provide additional functionality that can include anti-static, anti-microbial, self-cleaning and spectrally selective characteristics (Elvins, 2005; Gowenlock, 2014; Mabbett, 2011).

Spectrally selective coatings are formulated to provide thermal characteristics that often contradict intuitive associations of colour and temperature, i.e. dark and light coatings no longer have the greatest and lowest thermal build-up, respectively (Lavery, 2007). This is commonly achieved through the addition of various organic or inorganic pigments to the paint formulation that reflect a high percentage of infrared radiation, whilst transmitting a large portion of visible radiation (Fang, Kennedy, Futter, & Manning, 2013). An example of a spectrally selective coating that occurs naturally is chlorophyll, the pigmenting agent in plants responsible for their dark green colour. Chlorophyll allows plants to remain cool even in direct sunlight, a result of its high reflectance values within the infrared region (Lavery, 2007). Such coatings are gaining popularity in the construction industry where they can be applied to the external building system to aid in the control of the thermal build-up of the structure, whilst providing the desired aesthetics.

Pre-painted steels are produced in continuous, roll-to-roll processes at rates of up to 100 m min^{-1}, vital to the sustainability of which is the development of fast and energy efficient heating methods. Near-infrared (NIR) heating technology is a rapid radiative heating technique, capable of dramatically reducing a number of process times throughout roll-to-roll manufacturing, that has become a realistic option to cure coatings at elevated line speeds for the pre-painted steels market (Gowenlock, 2014; Mabbett, 2011; Mabbett et al., 2014; Watson, Mabbett, Wang, Peter, & Worsley, 2011). It is demonstrated in Mabbett (2011) that NIR technology is capable of reducing the cure time of a typical 15 μm polyester coating from ≈30 s achieved via conventional heating methods, to <10 s depending on the radiative properties of the coating.

Infrared emitters are characterised by the spectrum of radiation they emit, their operating temperatures and by their peak wavelengths of emission (Brogan & Monaghan, 1996; Cassidy, 1994). Typical NIR emitters utilise tungsten–halogen filaments, operate at colour temperatures of between 2000 and 3140 K and emit a broad spectrum of blackbody radiation. This radiation is primarily focused within the high energy density, near wave infrared subdivision of between 700 and 1400 nm. Heating is achieved by irradiating the coating with this broad spectrum of electromagnetic energy (Mabbett et al., 2014).

The thermal build-up within the furnace is a result of the absorption of the radiation received from the emitters. The extent of thermal build-up is related to the radiative properties of the coating, namely reflectance, absorptance and emissivity, and paints that vary in terms of these properties often display different heating rates to one another. This complicates the production process as coatings with different radiative properties achieve the cure temperature, around 500 K for

a typical polyester resin, at different exposure times. Strongly absorbing coatings can over-cure, whilst weakly absorbing coatings can under-cure, both of which result in unwanted surface defects that can lead to product failure within its agreed lifespan (Gowenlock, 2014; Mabbett, 2011).

The aim of this work was to develop a mathematical framework that can simulate the transient thermal behaviour of a spectrally selective coating within an NIR furnace. A standard finite difference thermal model connected with spectral radiative heat transfer as the heat source is presented, valid for a surface coating on any substrate. The input parameters are the reflectance spectrums of each coating, measured and imported directly using a spectrophotometer, and the basic material properties of the product such as thermal diffusivity, heat capacity and density. Good agreement is observed between experimental and simulated data. The model is of particular interest to the coating developer as a tool to simulate thermal behaviour without conducting expensive and time-consuming trials, to assess a coating's suitability to NIR curing and to gain an insight into process optimisation.

The structure of this paper is as follows. Section 2 gives an overview of the model, detailing the heat transfer mechanisms that are accounted for, the parameters investigated and the model assumptions. Section 3 is dedicated to providing a detailed overview of the governing formulae, the Monte Carlo procedure used to determine the radiation view factor, and the finite difference solution procedure. Finally, a description of the experimental method, measurement methodology and experimental validation is provided.

2. Model description

A schematic displaying the heat transfer mechanisms accounted for by the model and the radiation view factor geometry is given in Figure 1. The mechanisms are radiative heat transfer between the emitters and the product, radiative heat transfer between the furnace interior and the product and natural convective heat transfer between the furnace interior and the product. The six tungsten–halogen tube emitters are modelled as 2D infinite cylinders of radius r in parallel, separated by a distance h, and at a distance H from the product. The emitters and sample are positioned below and above a reflective panel, respectively. The reflectors are represented by the solid line in Figure 1. The model can account for coatings of different properties and gauge, variable emitter intensity, emitter to receiver distance, line speed, dwell time and heating above and/or below the product.

The analysis assumes that the emitting and receiving surfaces within the furnace are opaque, diffuse and grey. Only primary reflections are considered, and any secondary reflections from the reflector positioned above the heating area are not accounted for. At small aspect ratios, this can lead to an overestimate in the temperature; this is discussed in reference Lavery, Vujicic, and Brown (2005). The

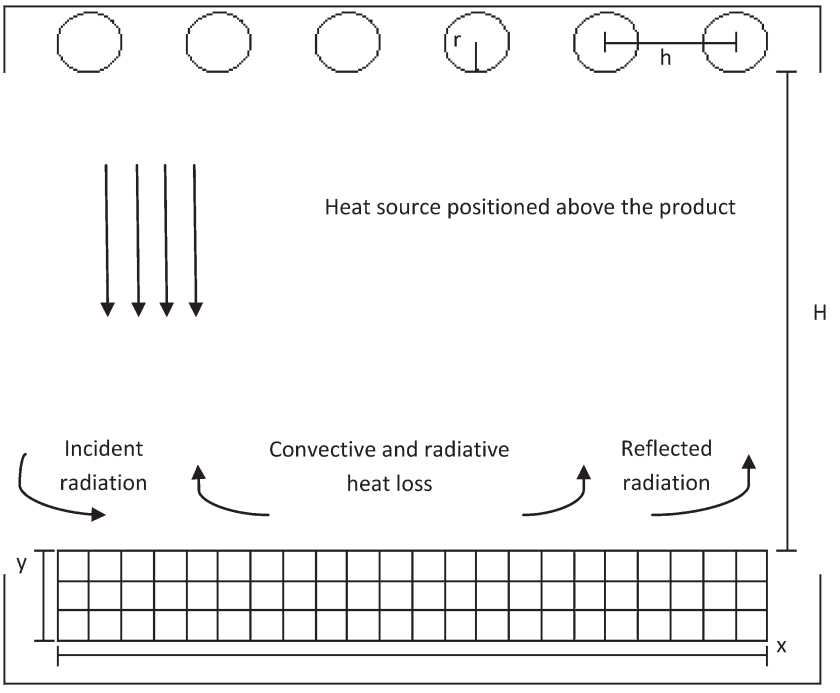

Figure 1. Schematic of the furnace geometry.

air and gas present within the furnace is non-participating and does not cause any loss in radiative flux intensity due to any absorption bands present.

3. Governing formulae

3.1. Incident radiation

Incident radiation received at the upper surface of the product is approximated as equivalent to a greybody. The colour temperature is a function of the emitter power input, measured as a percentage of maximal power input, and can be between T_c = 2000–3140 K with a total hemispherical grey emissivity of $\varepsilon_{\text{emitter}}$ = .17. Figure 2 shows the spectral energy distribution for T_c = 3140 K which is equivalent to a power input of 100%. This is in agreement with emission spectrums measured in Gowenlock (2014). For clarity, the electromagnetic spectrum is classified here as the ultraviolet spectrum (UV) 280–380 nm, the visible spectrum 380–740 nm, the NIR spectrum 740–1400 nm, the medium-wave infrared spectrum 1400–1500 nm and the far-wave infrared spectrum 1500–15000nm (Lavery, 2007).

Table 1 shows the percentage power input, equivalent colour temperature and peak wavelength of emission, calculated from Wien's law, for the furnace used in this study. At a maximum operating temperature of 3140 K, 50% of the emitted

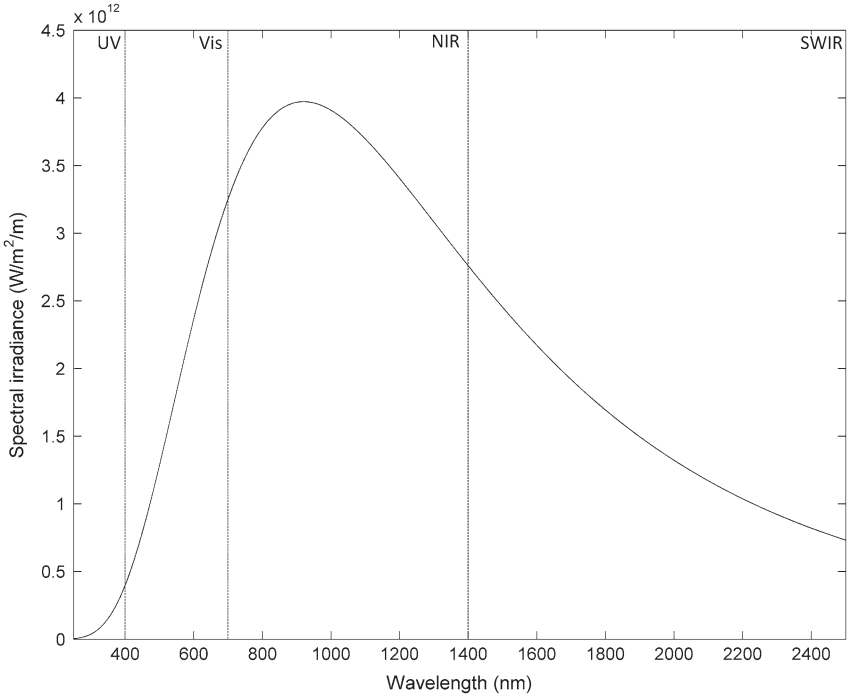

Figure 2. Spectral irradiance at 3140 K.

Table 1. Power input, colour temperature and peak wavelength of emission for Adphos 250 kW/m^2 NIR emitters.

Power input (%)	T_c (K)	λ_{max} (nm)
40	2240	1293.30
60	2600	1114.42
80	2890	1002.42
100	3140	923.03

energy is focused within the NIR region, with a peak wavelength of emission equal to $\lambda_{max} = 923.03$ nm.

Integrating the spectral energy distribution provided in Figure 2 gives the total irradiative flux that leaves the emitters; this is equal to the Stefan–Boltzmann equation given in Equation (1). Here, σ is the Stefan–Boltzmann constant, F_{ij} is the radiation view factor, A is the product's surface area and T_s is the temperature at the product's surface.

$$q_{\text{irradiation}} = \varepsilon_{\text{emitter}} \sigma F_{ij} A \left(T_c^4 - T_s^4 \right). \tag{1}$$

3.2. Radiation view factor

The radiation view (shape, configuration, form) factor F_{ij} is defined as the fraction of diffuse radiation leaving the finite surface A_i that is intercepted by the finite

surface A_j. The view factor is a function of the geometry of the system. The general expression is given by

$$F_{ij} = \frac{1}{A_i} \int_{A_i} \int_{A_j} \frac{\cos\theta_i \cos\theta_j}{\pi R^2} dA_i dA_j. \tag{2}$$

Exact solutions to Equation (2) are only possible for simple geometrical configurations. As the complexity of the system increases, analytical solutions become impractical and numerical techniques are required.

The view factor for the emitter and sample geometry seen in Figure 1 is determined numerically using the Monte Carlo ray tracing method. 'Monte Carlo' refers to a group of stochastic techniques that utilise random numbers generated to probability distributions to obtain numerical solutions. The basic characteristic, as applied here, is that the total energy emitted by a finite element is substituted with the emission of a total number of N rays where each ray carries the same amount of energy (Vujicic, 2006).

The origin of each ray is taken as the centre of the face of each element. Alternatively, a point on the element's face can be chosen at random; a study performed in Vujicic, Lavery, and Brown (2006) does not give precedence to either method. Sample points representing the angular displacement of each ray are chosen at random in the interval $[-\pi/2, \pi/2]$ to a cosine probability distribution to satisfy Lambert's law. The angular displacement is measured against the surface normal and is given by

$$\theta_d = \sin^{-1}(2 * random - 1), \tag{3}$$

where *random* is a uniformly generated random number in the interval [0, 1]. Figure 3 shows a typical ray vector **r**, emitted from a cylindrical filament of radius r at an angle θ_d relative to the surface normal **n**.

Tracing the paths of the N rays from surface i and recording the number of hits m on surface j, the radiation view factor becomes

$$F_{ij} = \frac{m}{N}. \tag{4}$$

An original computer program has been developed and tested against published analytical solutions. A number of geometries with varying degrees of complexity were considered, including infinite parallel plates and infinite parallel cylinders. Published analytical solutions can be found in Vujicic et al. (2006). The number of rays emitted from each element and the mesh resolution was varied and the resulting view factor compared to the corresponding analytical solution through

$$\delta(\%) = \frac{F_{ij(\text{numerical})} - F_{ij(\text{analytical})}}{F_{ij(\text{analytical})}} \times 100. \tag{5}$$

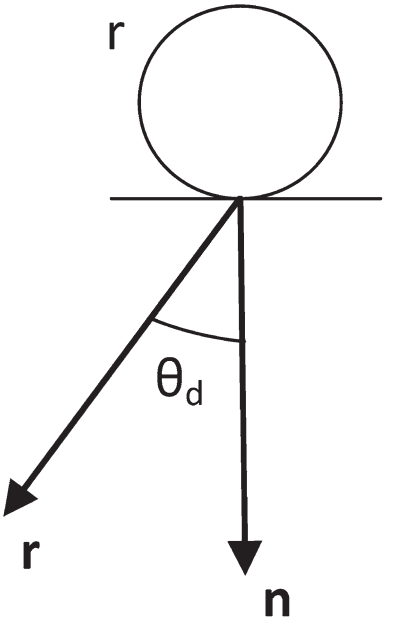

Figure 3. Schematic of ray vector r leaving emitter surface.

Numerical and analytical results for the case of the infinite parallel cylinders for 10, 20 and 40 surface elements can be seen in Table 2. Sample sizes of 100, 1000 and 10,000 rays per element were used, corresponding to a total number of between 1000 and 400,000 rays. Accuracy increases with ray sample size and as the number of surface elements is increased. Figure 4 shows the influence of the distance between the emitter and the receiver on accuracy; a greater ray sample size is required to compensate for a reduction in accuracy as this distance is increased.

It is worth noting that because values are obtained from a random number generator, values of the view factor can change from instance to instance even when the same geometric parameters and sample sizes are used. This is evident in Table 2 as sometimes high accuracy is observed from very small sample sizes.

Table 2. Numerical and analytical results for the case of the infinite parallel cylinders with $a = b = h = 1$.

Elements	Number of rays	Numerical solution	Analytical solution	δ (%)
10	100	.1090	.1107	−1.5321
	1000	.1108	.1107	.0940
	10,000	.1106	.1107	−.0777
20	100	.1130	.1107	2.0814
	1000	.1109	.1107	.1843
	10,000	.1106	.1107	−.0957
40	100	.1113	.1107	.5005
	1000	.1109	.1107	.1843
	10,000	.1108	.1107	.0917

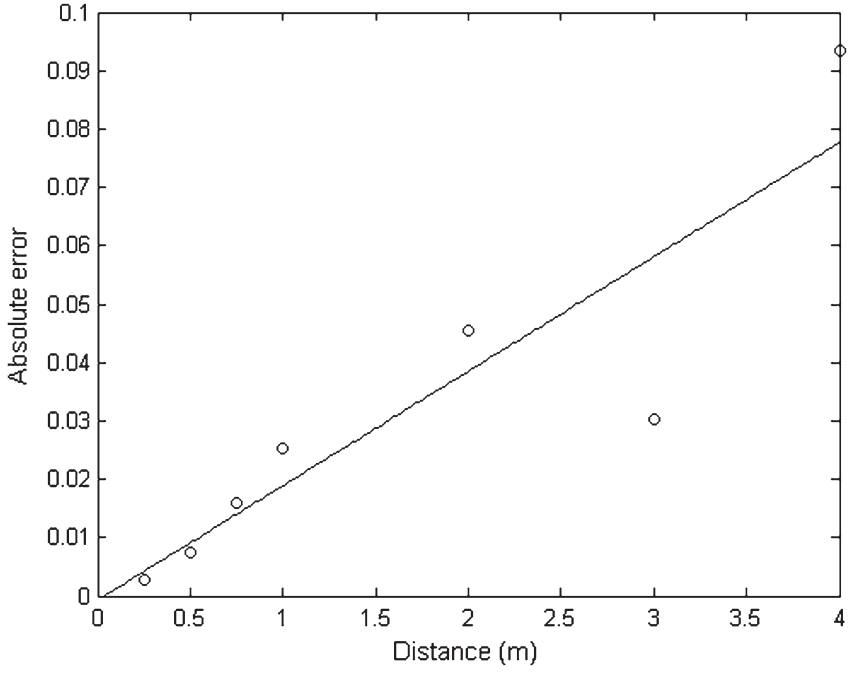

Figure 4. Absolute error against distance for the case of the infinite parallel cylinders with $a = b = 1$; 10 surface elements and a sample size of 1000 rays were chosen.

3.3. Reflected and absorbed spectral energy bands

For a spectral component of irradiation received at the product surface, fractions may be reflected, absorbed and transmitted. The coated substrate is largely opaque so it is assumed that no transmission occurs. The incident flux is separated into absorbed and reflected energy bands through the calculation of the total hemispherical reflectance coefficient, ρ, given by

$$\rho = \frac{\int_{\lambda_1}^{\lambda_2} \rho_\lambda(\lambda) E_{\lambda b}\left(\lambda, T_c\right) d\lambda}{\int_{\lambda_1}^{\lambda_2} E_{\lambda b}\left(\lambda, T_c\right) d\lambda}. \tag{6}$$

Here, $\rho_\lambda(\lambda)$ is the measured hemispherical spectral reflectance and $E_{\lambda b}(\lambda, T_c)$ is Planck's law for the emissive power of a blackbody given by

$$E_{\lambda b}\left(\lambda, T_c\right) = \frac{2\pi C_1}{\lambda^5\left(e^{\frac{C_2}{\lambda T_c}} - 1\right)}, \tag{7}$$

where T_c is the emitter operating temperature, λ is the wavelength and C_1 and C_2 are constants which can be found in Lavery (2007). The reflected and absorbed flux then become

$$q_{\text{reflected}} = \rho q_{\text{irradiation}}, \tag{8}$$

$$q_{\text{absorbed}} = (1 - \rho) q_{\text{irradiation}} . \tag{9}$$

3.4. Radiative heat losses

The surface re-radiates absorbed energy to the surroundings as it is being heated. Again, the net rate of heat transfer here is given by the Stefan–Boltzmann equation

$$q_{\text{radiation}} = \varepsilon_{\text{surface}} \sigma A \left(T_{\infty}^4 - T_s^4 \right) , \tag{10}$$

where T_{∞} is the ambient temperature and for a typical polyester, the total hemispherical emissivity is equal to $\varepsilon_{\text{surface}} = .89$, with coatings containing metallic flake having reduced values. For the surface temperatures experienced during the production process, only a very small portion of the radiated energy is within the NIR region.

3.5. Natural convective heat losses

Natural convection is described by Newton's law of cooling, which can be found in Vujicic et al. (2006). The average heat transfer coefficient $\bar{h}$ over the surface is estimated from the physical properties of air determined at a skin temperature T_f, defined as

$$T_f = \frac{T_{\infty} + T_s}{2} . \tag{11}$$

For air at atmospheric pressure and temperature T_f, values of the volume coefficient of expansion β, the kinematic viscosity υ, the thermal conductivity k and the Prandtl number Pr can be obtained from Table 3. The Rayleigh number Ra and Nusselt number Nu are determined from expressions found in DeWitt et al. (2007). Note that the Nusselt number is a function of the Rayleigh number and the form of its expression depends on the orientation of the surface. The heat transfer coefficient for the system is then obtained from

$$\bar{h} = \frac{kNu}{L}. \tag{12}$$

Table 3. Temperature-dependant thermal properties of air at atmospheric pressure, taken from Vujicic et al. (2006).

T_s (K)	β (K^{-1})	υ (10^{-6} m^2s^{-1})	k (W/mK)	Pr
300.00	.0333	15.89	.0263	.707
350.00	.0029	20.92	.0300	.700
400.00	.0025	26.41	.0338	.690
450.00	.0022	32.39	.0373	.686

Table 4. Values for the Nusselt number, Rayleigh number and convective coefficient.

T_s (K)	T_f (K)	Ra ($\times 10^9$)	Nu horizontal	Nu vertical	$\bar{h}$ horizontal (W/m^2)	$\bar{h}$ vertical (W/m^2)
300.00	296.50	.64	112.78	10.33	2.97	.27
350.00	321.50	2.55	178.01	12.79	5.34	.38
400.00	346.50	2.59	178.94	12.81	6.05	.43
450.00	371.50	2.21	169.82	12.49	6.33	.46

Values for the convective coefficient for a range of surface temperatures and for an ambient temperature of $T_\infty = 293$ K are given in Table 4.

3.6. Governing equations

The two-dimensional time-dependent conduction heat transfer equation is given by

$$\rho C_p \frac{\partial T}{\partial t} - k\left(\frac{\partial^2 T}{\partial x^2} + \frac{\partial^2 T}{\partial y^2}\right) = Q, \tag{13}$$

where T is the temperature, t is time, ρ is the density, C_p is the specific heat capacity and k is the thermal conductivity. The surface boundary condition Q is given by Equations (14) and (15) for the upper and lower surfaces, respectively.

$$Q_{\text{upper}} = q_{\text{absorbed}} + q_{\text{convection}} + q_{\text{radiation}}\,. \tag{14}$$

$$Q_{\text{lower}} = q_{\text{convection}} + q_{\text{radiation}}\,. \tag{15}$$

The initial condition that governs the partial differential equation is

$$T(x, y, t) = T_\infty \text{ at } t = 0. \tag{16}$$

An explicit forward-time central-space (FTCS) finite difference solution is used. The time derivative is replaced with a forward difference expression and the spatial derivative is replaced with a central difference expression given in Equation (17). The FTCS scheme is conditionally stable and it was necessary to linearise the Stefan–Boltzmann equation through the radiative heat transfer coefficient h_r.

$$\frac{\partial T}{\partial t} = \frac{T_{i,j}^{n+1} - T_{i,j}^{n}}{\Delta t}\,, \tag{17}$$

$$\frac{\partial^2 T}{\partial x^2} = \frac{T_{i+1,j}^{n} - 2T_{i,j}^{n} + T_{i-1,j}^{n}}{\Delta x^2}\,, \quad \frac{\partial^2 T}{\partial y^2} = \frac{T_{i,j+1}^{n} - 2T_{i,j}^{n} + T_{i,j-1}^{n}}{\Delta y^2}\,.$$

4. Reflectance data

The hemispherical spectral reflectivity was obtained for a range of industrially applied coloured polyester coatings provided by BASF. A Perkin Elmer UV/Vis/NIR 700 Spectrophotometer with a 60 mm integrating sphere was used to determine the reflectivity within the 250 to 2500 nm wavelength band and a Perkin Elmer Spotlight 400 FT-IR Imaging System was used to determine the reflectivity within the 2500 to 15000 nm wavelength band. Test measurements were performed in accordance with ASTM Standard Test Method E903-96.

Steel substrate panels measuring $100 \times 200 \times .85$ mm were coated via the bar method described in Mabbett (2011) with a 15 μm polyester and cured in a convection oven at 504.15 K for 45 s. Measured spectral data can be seen in Figures 5 and 6. The samples are labelled according to their colour as Black, IR Black, Brown, IR Brown, Silver and White. The IR Black and IR Brown coatings are spectrally selective and contain IR reflective pigments; these coatings exhibit greater reflectance values within the IR regions whilst maintaining similar values in the visible region. Note that coatings are available in an almost unlimited number of hues; as a result, reflectance values may vary from other arbitrarily selected coatings of similar colour description.

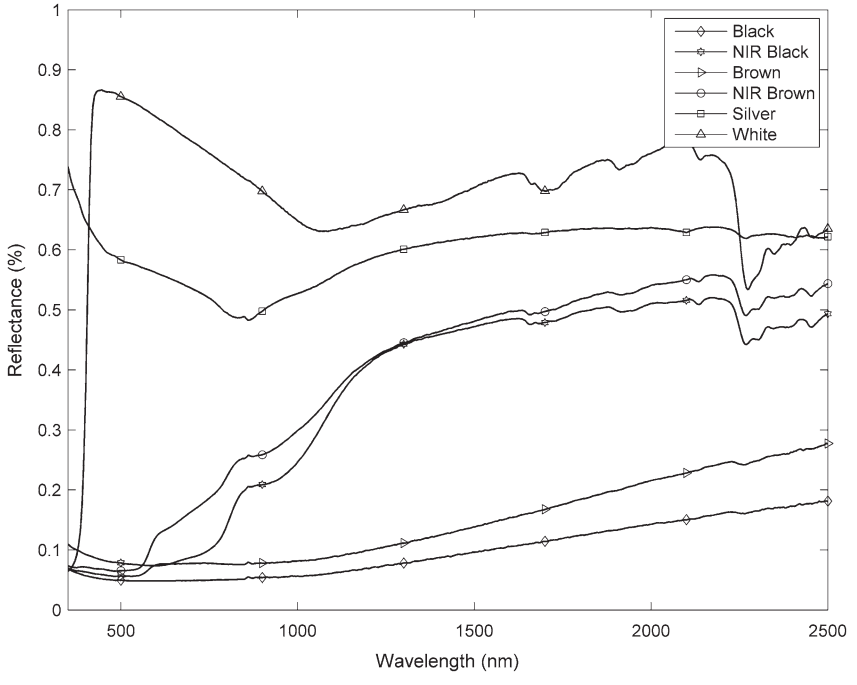

Figure 5. Reflectance spectra for coloured polyester coatings in the 250–2500 nm wavelength band.

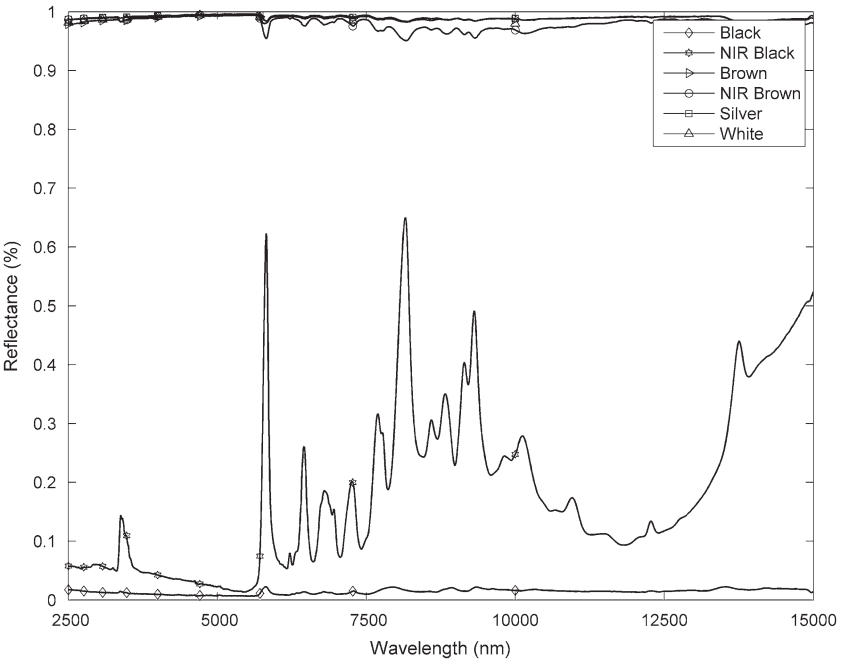

Figure 6. Reflectance spectra for coloured polyester coatings in the 2500–15000 nm wavelength band.

5. Results

The model was used to simulate the temperature profiles of steel substrate panels coated with the polyesters whose reflectance spectra were determined in Section 4. The furnace used was an Adphos NIR Lab Unit with 250 kW/m^2 emitters. The reflectance and absorptance coefficients were determined by following the procedure described in Section 3.3. Via the bar method, 15 μm coatings were applied to substrate panels measuring $100 \times 200 \times .85$ mm. The emitter power input was 60% which equates to a colour temperature of 2600 K. Temperature measurements were taken with a K-type thermocouple spot welded to the centre rear of the coated panel and recorded using a TC-08 data logger to an accuracy of ±.75%. Table 5 shows the absorption and reflectance coefficients for the coatings and the simulated and measured peak temperatures for a 4 s exposure. Figure 7 gives the simulated temperature profiles during heating.

Lighter coatings such as White and Silver show the greatest reflectance and lowest absorptance coefficients, whilst the darker Black and Brown coatings show the lowest reflectance and greatest absorptance coefficients. Black and White coatings represent maximum and minimum absorptance values, respectively, whilst other paints fall in between these extremities. The model is in good agreement with experimental data, with the thermal behaviour of the coatings following the order of reflectance; coatings with the lowest reflectance coefficients display the greatest heating rates. The model accounts for the variation in the reflectance values of the

Table 5. The total reflectance ρ, total absorptance α, predicted T_s and measured T_m, temperatures after an exposure of 4 s.

	ρ	α	T_s (K)	T_m (K)
Black	.09	.91	376.20	365.99
IR Black	.39	.61	350.78	339.91
Brown	.16	.84	370.23	357.92
IR Brown	.37	.63	352.47	351.70
Silver	.58	.42	334.67	338.79
White	.69	.31	325.35	321.54

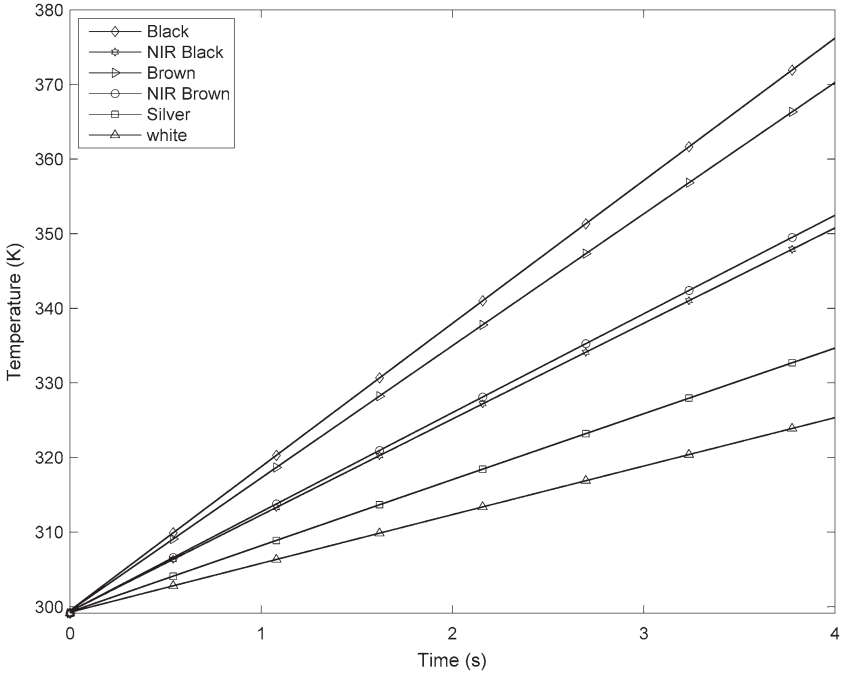

Figure 7. Simulated temperature profiles of coloured polyesters for a 4 s exposure.

IR Black and IR Brown coatings, with these paints displaying a deviation in their reflectance coefficients and heating rates when compared to their non-spectrally selective counterparts due to the addition of IR reflective pigments. Both the IR Black and IR Brown coatings reach peak temperatures of approximately 20 K below the standard Black and Brown formulations. The variability of heating rates between each coating suggests that process speeds could be optimised with respect to a coatings reflectance coefficient. It is observed that the Black coatings could reach a cure temperature of 500 K much faster than a white coating, possessing a heating rate approximately three times greater.

6. Future work

The model will be expanded to account for successive reflections within the furnace; this function will be used to describe reflectors that can be used increase

the effectiveness of the heating. The ability to simulate more complex extraction systems will also be introduced by coupling the model with CFD to describe forced convective heat transfer.

Current work has focused on simulating transient thermal behaviour; this will be developed further to simulate the NIR flux and temperature distribution across the product surface. Ensuring temperature uniformity during the manufacturing process is vital to a product's finished quality and longevity.

7. Conclusions

A transient finite difference thermal model connected with blackbody equivalent spectral radiative heat transfer as the heat source is presented, valid for spectrally selective surface coatings on any substrate within a NIR furnace. The model is validated against a range of coloured polyester coatings and good agreement is observed between experimental and simulated data. The expected relationship between colour and absorption is displayed, with darker coatings displaying greater absorption and heating rates than lighter coatings. Surprisingly, colours which appear similar to one another can display different heating rates, a result of their different infrared absorption properties. This is demonstrated through the spectrally selective coatings IR Black and IR Brown. The ultra-fast heating potential of NIR technology is demonstrated effectively, with coatings heating at a much faster rate than with conventional curing technology. The variability of heating rates between coatings of different radiative properties suggests that process speeds could be optimised with respect to these properties.

Acknowledgements

The authors would like to acknowledge Swansea University, Tata Steel Colors, The Engineering and Physical Sciences Research Council (EPSRC) and the Welsh Government for supporting and funding this body of work.

Disclosure statement

No potential conflict of interest was reported by the authors.

Funding

This work was supported by Engineering and Physical Sciences Research Council [EP/K503228]; European Social Fund.

ORCID

D. A. Brennan http://orcid.org/0000-0002-1732-7654

References

Brogan, M. T., & Monaghan, P. F. (1996). Thermal simulation of quartz tube infra-red heaters used in the processing of thermoplastic composites. *Composites Part A: Applied Science and Manufacturing, 27*, 301–306.

Cassidy, S. F. (1994). *Mathematical modelling of infrared heating of thermoplastic composites in diaphragm forming* (PhD Thesis). University College Galway, Galway.

DeWitt, D. P. , Incropera, F. P., Bergman, T. L., & Lavine, A. S. (2007). *Fundamentals of heat and mass transfer* (6th ed.). Hoboken, NJ: Wiley.

Elvins, J. (2005). *The relationship between the microstructure and corrosion resistance of Galfan coated steels* (EngD Thesis). College of Engineering, Materials Research Centre, University of Wales Swansea, Swansea.

Fang, V., Kennedy, J., Futter, J., & Manning, J. (2013). A review of infrared reflectance properties of metal oxide nanostructures. *GNS Science Report, 39*, 23 p.

Gowenlock, C. (2014). *Near infrared curing of high performance coil coatings* (EngD Thesis). College of Engineering, Materials Research Centre, Swansea University, Swansea.

Lavery, N. P. (2007). Mathematical framework for predicting solar thermal build-up of spectrally selective coatings at the Earth's surface. *Applied Mathematical Modelling, 31*, 1635–1651.

Lavery, N. P., Vujicic, M. R., & Brown, S. G. R. (2005). Thermal experimental investigation of radiative heat transfer for the validation of radiation models. *CMEM, 41*, 251–261. ISSN1743-355X.

Mabbett, I. (2011). *Applications of near infrared heating of interest to the coil coating industry* (EngD Thesis). College of Engineering, Materials Research Centre, Swansea University, Swansea.

Mabbett, I., Elvins, J., Gowenlock, C., Glover, C., Jones, P., Williams, G., & Worsley, D. A. (2014). Addition of carbon black NIR absorber to galvanised steel primer systems: Influence on NIR cure of polyester melamine topcoats and corrosion protection characteristics. *Progress in Organic Coatings, 77*, 494–501.

Vujicic, M. R. (2006). *Finite element modelling and experimental validation in radiative heat transfer* (PhD Thesis). School of Engineering, University of Wales Swansea, Swansea.

Vujicic, M. R., Lavery, N. P., & Brown, S. G. R. (2006). Numerical sensitivity and view factor calculation using the Monte Carlo method. *Proceedings of the Institution of Mechanical Engineers, Part C: Journal of Mechanical Engineering Science, 220*, 697–702.

Watson, T., Mabbett, I., Wang, H., Peter, L., & Worsley, D. A. (2011). Ultrafast near infrared sintering of TiO_2 layers on metal substrate for dye-sensitized solar cell. *Progress in Photovoltaics: Research and Applications, 19*, 482–486.